Measurement of interfacial shear (friction) with an ultrahigh vacuum atomic force microscope

R. W. Carpick
Materials Sciences Division, Lawrence Berkeley National Laboratory, Berkeley, California 94720 and Department of Physics, University of California at Berkeley, Berkeley, California 94720

N. Agraït,[a] D. F. Ogletree, and M. Salmeron
Materials Sciences Division, Lawrence Berkeley National Laboratory, Berkeley, California 94720

(Received 24 July 1994; accepted 22 November 1995)

We have studied the variation of frictional force with externally applied load for a Pt-coated atomic force microscope tip in contact with the surface of mica cleaved in ultrahigh vacuum. At low loads, the frictional force varies with load in almost exact proportion to the area of contact as predicted by the Johnson–Kendall–Roberts (JKR) theory [K. L. Johnson, K. Kendall, and A. D. Roberts, Proc. R. Soc. London Ser. A **324**, 301 (1971)] of elastic adhesive contacts. The friction-load relation for a deliberately modified tip shape was proportional to an extended JKR model that predicts the area-load relation for nonparabolic tips. The tip shape was determined experimentally with a tip imaging technique and was consistent with the predicted friction behavior. This demonstrates that the frictional force is proportional to the area of contact between the tip and sample. Using the JKR/extended JKR model, interfacial surface energies and shear strengths can be estimated.

I. INTRODUCTION

The study of adhesion, friction, and wear between interacting surfaces in relative motion, described today as the field of tribology, has been a ripe area of study for centuries.[1] Recent experimental advances such as the surface forces apparatus (SFA),[2–5] the quartz–crystal microbalance[6–8] and the atomic force microscope (AFM)[9,10] have extended these studies to the atomic and molecular level. These techniques show promise to provide a fundamental understanding of tribological phenomena at the atomic scale.

One important case where frictional forces arise is the wearless sliding interface between two materials where only elastic deformation takes place. Bowden and Tabor recognized early on in their wide-ranging studies of friction[11] that adhesion between materials can contribute to friction, independent of contributions due to the ploughing of surface asperities. Further work with the SFA[12,13] has explored wearless friction between flat surfaces (mica is most commonly used), often with confined molecular layers in between. Unfortunately, there is a limited choice of substrates with SFA, and experiments are usually restricted to pressures <10 MPa, with some exceptions.[14] Furthermore, SFA has a limited lateral spatial resolution of roughly a few square microns. However, the SFA does possess the advantage that the contact area can be directly measured.

The AFM, in contrast, can measure both normal and lateral forces with atomic-scale contrast.[10] Microfabrication techniques can produce sharp tips with tip radii <1000 Å. If externally applied loads are kept low, then the AFM tip forms a nanometer-sized single asperity contact with the surface being probed, and interaction forces can be measured without causing plastic deformation. One drawback of this technique is that the contact area cannot be directly measured, and is difficult to infer unless the exact tip shape is known. Furthermore, to actually calculate forces, the AFM lever constants must be known, which is a nontrivial measurement to perform. Finally, the exact chemical nature of the interface is not known since contamination may be present.

To overcome the last difficulty, we have constructed an ultrahigh vacuum (UHV) AFM[15] where surfaces can be cleaved or prepared and then probed *in situ*.

To address the question of signal calibration, we have devised methods to directly measure the normal and lateral lever force constants, but that will be discussed in a longer article elsewhere.[16] For this work, we will rely upon estimates of lever constants. However, we will show that a significant amount of information can be gained without an exact calibration of the AFM signals.

There is no way at present to directly measure the tip–surface contact area with a conventional AFM. However, the tip shape can be determined with some precision using a suitable sample, described below. We will show that measurable differences in frictional behavior can be associated with different tip sizes and shapes.

For this set of experiments, we will investigate the frictional behavior of Pt-coated AFM tips in contact with a bare mica surface in UHV.

II. THEORETICAL BACKGROUND

There have been a number of continuum models of contact mechanics developed to describe the elastic contact between two bodies, the pioneering work being done by Hertz.[17] The Hertzian model does not take into account at-

[a]Permanent address: Instituto Universitario de Ciencia de Materiales "Nicolás Cabrera," Laboratorio de Bajas Temperaturas, C-III, Universidad Autónoma de Madrid, 28049 Madrid, Spain.

tractive forces between the contacting surfaces. One such model which takes surface forces into account is due to Johnson, Kendall, and Roberts (JKR).[18] The JKR theory considers the effect of finite surface energy on the properties of the interface. In particular, the theory calculates the increase in contact area that results from the elastic bodies deforming to accommodate their mutual attraction, so that the deformations are no longer perfectly Hertzian. The initial formulation of the theory was applied to the case of two spheres (approximated as paraboloids) in contact, which is equivalent to a sphere-plane contact by considering one sphere to have an infinite radius. The model can be extended to more general shapes.[19,20]

The general features of the JKR theory are as follows. The surfaces are considered to possess a finite surface energy per unit area $\gamma=\gamma_1+\gamma_2-\gamma_{12}$, where γ_1 and γ_2 are the respective surface energies and γ_{12} the interfacial energy. The terms γ is equivalent to the Dupré energy of adhesion and corresponds to the work per unit area required to separate the surfaces from contact to infinity. The contact area A as a function of externally applied load L is given by

$$A^{\frac{3}{2}}=\frac{\pi^{\frac{3}{2}}R}{K}\cdot[L+3\pi R\gamma+\sqrt{6\pi R\gamma L+(3\pi R\gamma)^2}], \tag{1}$$

where R is the tip radius and K is the reduced modulus of the two materials, given by

$$K=\frac{4}{3}\left(\frac{1-\nu_1^2}{E_1}+\frac{1-\nu_2^2}{E_2}\right)^{-1}, \tag{2}$$

with E_1 and E_2 the respective Young's moduli, and ν_1 and ν_2 the respective Poisson ratios. The Hertz formula is recovered by setting $\gamma=0$. At zero applied load, there is a finite contact area given by

$$A_0=\pi\left(\frac{6\pi\gamma R^2}{K}\right)^{\frac{2}{3}}. \tag{3}$$

Furthermore, a finite negative load is required to separate the surfaces. This value is often referred to as the critical load and is given by

$$L_c=-\tfrac{3}{2}\pi R\gamma. \tag{4}$$

This is equivalent to the pull-off measured in AFM experiments (if the tip is truly parabolic). At the critical load, a finite contact area exists. We shall refer to this area as the critical area, A_c, and is equal to $2^{-\frac{4}{3}}A_0$.

SFA experiments with contacting mica surfaces having either contaminant or liquid layers between them have shown that in the absence of wear, the frictional force F_f is directly proportional to the contact area,[21] i.e.,

$$F_f=\tau A, \tag{5}$$

where τ is the shear strength. Note that this means there will be a finite frictional force at the pull-off point, which we shall call the critical friction, F_c, given by

$$F_c=\tau A_c=\pi\tau\left(\frac{3\pi\gamma R^2}{2K}\right)^{\frac{2}{3}}. \tag{6}$$

The JKR equation can then be rewritten in the following compact nondimensional form:

$$\hat{F}_f=(1+\sqrt{1+\hat{L}})^{\frac{4}{3}}, \tag{7}$$

where the load and friction have been parametrized in terms of the critical load and critical friction

$$\hat{F}_f=\frac{F_f}{F_c}\quad\text{and}\quad\hat{L}=\frac{L}{|L_c|}. \tag{8}$$

The above discussion shows that although four physical quantities are involved in the friction-load equation (surface energy, tip radius, modulus, and shear strength), there are only two adjustable parameters in the equation: L_c [Eq. (4)] and F_c [Eq. (6)]. These two quantities [or any other pair of values (L,F) on the curve] determine the scale of the JKR friction curve.

All of these equations are only valid for parabolic tip profiles. Treating the tip as a perfect sphere introduces a negligible correction except for very large contact areas.[20] However, a nonparabolic tip shape produces substantially different behavior. We have extended the JKR model to predict the contact area for an axisymmetric tip with a general power law height profile $(z=c\cdot r^n)$. The result is given in the Appendix. The extended JKR equation is used for various values of n in Figs. 1 and 3. In general, a flatter tip profile, such as a quartic tip $(z\sim r^4)$ produces an area-load relation with substantial qualitative differences. Particularly, the area does not increase as rapidly with externally applied load as in the case of a parabolic tip. This is intuitively obvious as the limiting case is that of a flat cylindrical punch; the contact area would be independent of load due to the flat tip profile. Yet for different tip shapes, it is still true that there will be a nonzero pull-off force and a finite contact area at pull off, and the modified area-load relation can still be written in terms of these two parameters.

Thus, a set of friction versus load measurements acquired from some positive load all the way down to pull off will allow one to distinguish between different possible tip shapes, and the interfacial energy and shear strength can then be determined.

III. EXPERIMENT

A. Sample and tip preparation

The mica surface is held fixed in a sample holder inside the UHV chamber; the exact arrangement is described elsewhere.[16] A thin steel foil is epoxied on top of the mica sample and protrudes outward far enough to be grabbed by a wobble stick. Using the wobble stick, the foil is pulled off and carries a few layers of mica with it, exposing a fresh mica surface. The AFM is then brought into range to perform the experiment.

The experiment was performed with a single Si_3N_4 cantilever[22] which was coated with 1000 Å of Pt. The Pt was

deposited after a brief plasma etch of the lever to ensure good adherence. To determine if the tip was truly Pt terminated, we placed the tip in contact with a conducting sample and measured a low contact resistance (1.5 kΩ including lead resistance) both before and after acquiring all the data described below. The resistance did not vary appreciably with applied load, even just before pull off. Since Si_3N_4 is an insulator, we conclude that throughout the experiment, the Pt coating was not removed.

The chamber pressure during the friction experiments was 5×10^{-10} Torr or less, and all experiments were performed with the system at room temperature.

B. Tip shape determination

An AFM image is actually a convolution of surface and tip features. The smaller and sharper the features of one, the more the AFM image corresponds to the topography of the other. Usually, one hopes for sharp AFM tips to reveal the surface topography, but equivalently, a sharp surface feature will reveal the tip structure. Several methods have been discussed recently[23–26] that allow the AFM tip profile to be imaged based on this principle. However, in general the finite lateral extent of the surface feature will increase the apparent size of the tip. Thus, the ''tip images'' acquired by these methods are in fact the largest possible tip that could have produced the image, meaning that these methods provide upper bounds on the tip dimensions.

One useful surface for the purpose of tip imaging is the stepped $SrTiO_3(305)$ surface proposed by Sheiko *et al.*[27] Once annealed, the surface terminates in a large number of (101) and (103) facets which form long sharp ridges that are suitable for tip imaging. Since the step density is high, acquired images contain many individual tip images which can be averaged to reduce the effect of noise and spurious surface features. The (101) and (103) facets of the $SrTiO_3$ surface are inclined with respect to the surface plane by $+14°$ and $-12.5°$, respectively. The tip apex is imaged when the tip contacts the crest of the ridge. Thus, only the end portions of the tip that are less steep than the ridges will be imaged by this technique.

Since we would like to have some measure of the tip shape and dimensions, we imaged the tip with $SrTiO_3(305)$ before and after each full set of data. These measurements were performed in air. Since the ridges are extended, the image provides only a one-dimensional cross section of the tip along the scanning direction. However, we could reorient the surface and scan in the perpendicular direction to obtain the perpendicular tip cross section. No substantial asymmetry was observed with this tip. All references to tip shape and size were obtained by this method. Although these measurements are actually upper bounds to the tip dimensions, there was no substantial difference between tip images acquired on different ridges. This suggests, in combination with transmission electron microscopy (TEM) images of the $SrTiO_3(305)$ surface[27] and the high elastic modulus of $SrTiO_3$, that the apparent dimensions are not grossly different from the true ones as the ridges are very sharp and rigid.

C. Data acquisition

To acquire a set of friction measurements at different applied loads, we simultaneously measure the normal and lateral bending of the AFM cantilever as it is scanned laterally across the surface for a series of applied loads.[28] The normal bending signal is directly proportional to the externally applied load. The average value of the difference in maximum lateral signal acquired scanning left to right and then right to left is proportional to the frictional force. These measurements can be performed over any desired load range. For these experiments, we usually begin the measurements at a substantial positive load which is decreased until the tip pulls out of contact with the surface. No significant difference is observed if the data is acquired while increasing the load except that, due to the jump-to-contact instability, the low load portion of the friction versus load curve is inaccessible.

At very high loads, anomalously large lateral forces occur indicating the onset of wear of the mica surface, similar to effects seen in air.[28] For these experiments, all friction data were obtained with the externally applied load remaining well below the wear threshold.

IV. RESULTS AND DISCUSSION

Figure 1 shows a characteristic friction versus load plot for the Pt-coated tip on mica in UHV. The data are plotted in (estimated) nanonewtons. The x axis corresponds to externally applied load, i.e., normal cantilever displacement with respect to zero bending. The zero point is given by the cantilever position out of contact with the sample when no normal force is acting. The behavior is nonlinear with the nonlinearity most evident near pull off. Clearly, there is a finite frictional force at the pull-off point. The critical load that results while scanning laterally corresponds with the pull-off force measured from force-distance curves that are acquired without lateral scanning, but are often of smaller magnitude. These ''premature'' pull-off events may be due to increased instabilities during scanning, or may be a consequence of the influence of lateral forces on the interface.[29] This effect will be discussed in more detail elsewhere.[30]

Figure 1 also shows the three JKR or extended JKR curves overlaid for comparison. The three curves correspond to successively flatter axisymmetric tip profiles of $z\sim r^2$, r^4, and r^6, respectively, all fit to the critical load and the friction at zero load. Clearly, only the parabolic tip suits the data, and it does so very accurately. One can see that the data cannot be fit by the $z\sim r^4$ and r^6 solutions as they predict friction values too large at negative loads, and too small at positive loads. The disagreement is a consequence of the shape of the curve, as opposed to the relative calibration of the axes. Thus, we can determine whether or not the JKR or extended JKR equations fit the data independent of the absolute calibration of the cantilever forces.

Before these data were taken, the tip was imaged using the $SrTiO_3(305)$ surface. An averaged tip profile is shown in Fig. 2. The profile is fit well by a parabola with a radius of curvature of 140 nm. The parabolic profile agrees with the JKR fit to the friction data.

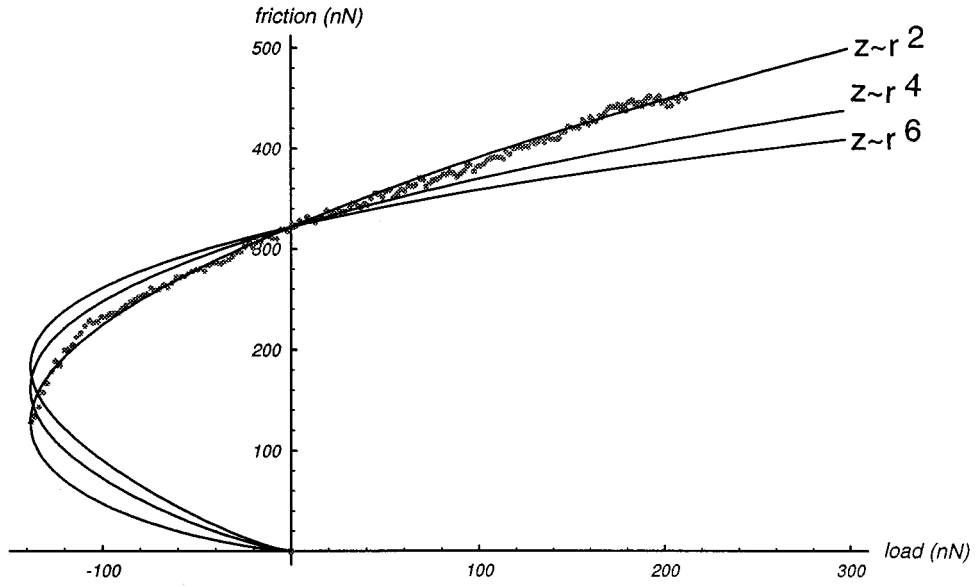

FIG. 1. A characteristic friction vs load plot for a Pt-coated tip on mica in UHV (gray dots). The x axis corresponds to externally applied load, i.e., normal cantilever displacement. The zero point is given by the normal cantilever displacement out of contact with the sample. The pull off occurs at a load of -138 nN. Note the nonlinear dependence of friction with load, and the finite frictional force at the pull-off point. The three solid lines are JKR or extended JKR curves for the following tip profiles: $z\sim r^2$, r^4, and r^6. The three curves are fit to the critical load, and to the value of the friction at zero applied load to match the acquired data. The $z\sim r^2$ curve fits the data extremely well.

To further investigate the validity of the JKR or extended JKR models, we decided to study the behavior of a substantially different tip shape and see if the friction versus load behavior changed accordingly. Since the Pt coating is relatively thick (nominally $\sim$1000 Å), we attempted to deliberately alter the tip shape by exerting large forces on the tip. This was done by exerting an extremely high load of $\sim$1000 nN on the tip, corresponding to an estimated average pressure of roughly 60 GPa, then reducing the load somewhat to $\sim$500 nN, and then scanning the tip across the surface $\sim$20 times. Friction data was then acquired at the usual applied loads. Figure 3 shows one of the resultant friction versus load plots, accompanied by fits for the same three tip profiles as before; $z\sim r^2$, r^4, and r^6, with the r^8 solution added for further comparison. Now the r^6 profile provides a good fit. In fact, the r^8 solution fits the data well in the negative load region. This clearly indicates that the end of the tip is indeed flatter than before. There was some evolution of the data as we continued to perform the scans. The details of this behavior will be reported elsewhere,[31] but we note that none of the data from subsequent scans reverted to the behavior expected for sharper tip profiles.

After these data were acquired, we again imaged the tip using the $SrTiO_3(305)$ surface. This time, a much flatter tip profile was observed. Figure 4 displays the cross section from the ''blunted'' tip and the original tip plotted on the same scale, along with $z\sim r^4$ and r^6 profiles. As mentioned above, the tip profiles obtained from the $SrTiO_3(305)$ sample are limited to the end portion of the tip where its profile is less steep than the $SrTiO_3$ ridges. The analysis is also complicated by the fact that the ridge may not to be perfectly sharp. However, we estimate using the JKR/extended JKR theory that the indentations at maximum load were approximately 7 Å. Thus, only the last few Å of the tip profile need to be considered to understand, at least approximately, the elastic behavior. In this case, $z\sim r^6$ is a suitable fit to the data, consistent with the friction-load data presented in Fig. 3. In fact, the tip shape could certainly be described to greater accuracy by a more complicated function for which

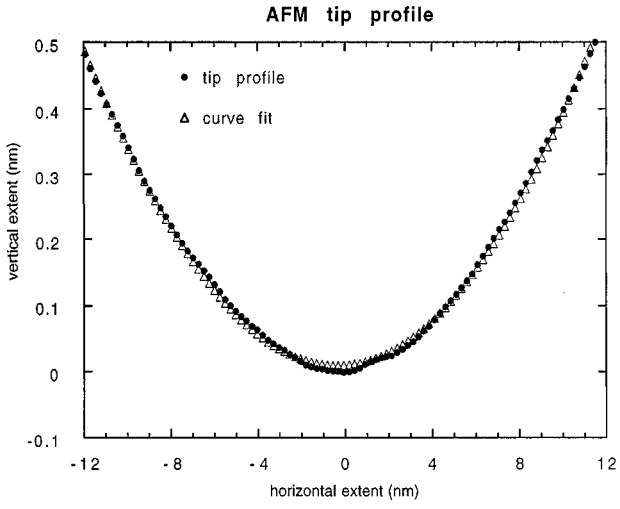

FIG. 2. A tip image acquired from scanning the $SrTiO_3(305)$ surface in air, taken before the tip was placed in vacuum and the data in Fig. 1 acquired. The actual tip profile is plotted with solid circles, and a parabolic fit is plotted with open triangles for comparison. The tip profile is essentially parabolic, with an effective tip radius of $\sim$140 nm.

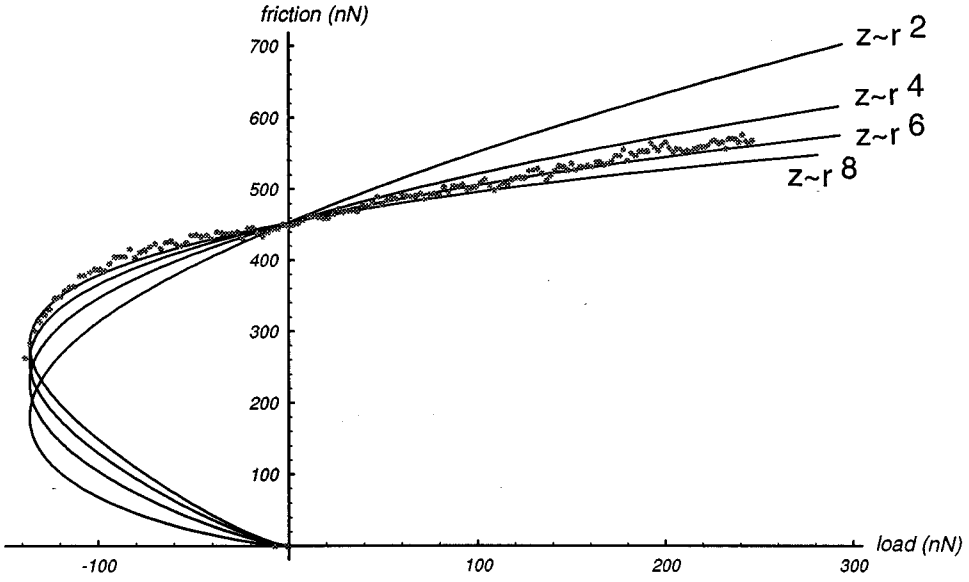

FIG. 3. Friction vs load data (gray dots) for the Pt-coated tip after it was deliberately blunted. The four solid lines are JKR or extended JKR curves for the following tip profiles: $z \sim r^2$, r^4, r^6, and r^8. As before, all curves are fit to the critical load, and the friction at zero applied load to match the acquired data. This time, the $z \sim r^6$ curve fits the data best, consistent with a flatter tip profile.

an area-load curve could be worked out for comparison to the data, but that is not the main point of this work. We simply assert that the tip is qualitatively much flatter than before, and that this corresponds to the change in frictional behavior we observed after the tip was blunted. Furthermore, the $z \sim r^6$ solution is seen to be a reasonable estimate of the tip shape, consistent with both the tip imaging technique and the friction versus load data. Calculations based upon this estimate of the tip shape are not significantly affected by considering more exact mathematical descriptions.

The above results show that the variation of our friction data with load is described to an excellent degree by JKR/extended JKR model depending on the tip shape. These models predict contact area as a function of load, which indicates that the frictional force between Pt-terminated AFM tips and the mica surface is proportional to the area of contact. We have also performed experiments with a lever and tip fabricated from Si and Si_3N_4. These experiments also produced frictional forces that are proportional to the JKR/extended JKR model for contact area. The results with Si and Si_3N_4 tips will be discussed elsewhere.[30]

As mentioned, shear strength relates frictional force to contact area. A pressure-dependent shear strength has been observed for carboxylic acid layers between mica surfaces in a SFA experiment.[14] Our data indicate direct proportionality between contact area and frictional force which would imply a pressure-independent shear strength over the pressure range we attained, up to ~0.7 GPa average pressure.

For each set of data, the theoretical equation corresponding to the appropriate tip shape can be determined and verified with tip imaging. For example, the curve in Fig. 1 is described by the JKR equation for a parabolic tip, Eq. (8). Fitting the equation to the data gives values for F_c and L_c so long as the load and friction forces are properly calibrated. As mentioned, a more accurate calibration of AFM signals will be discussed in a future article.[16] The following calculations are based on approximate calibrations, but we perform them to illustrate the point that in principle these calculations can be done, and that even our estimates constitute interesting results.

To perform these calculations, we used a Young's modulus of 177 GPa for Pt[32] and 56.5 GPa for the mica *c* axis,

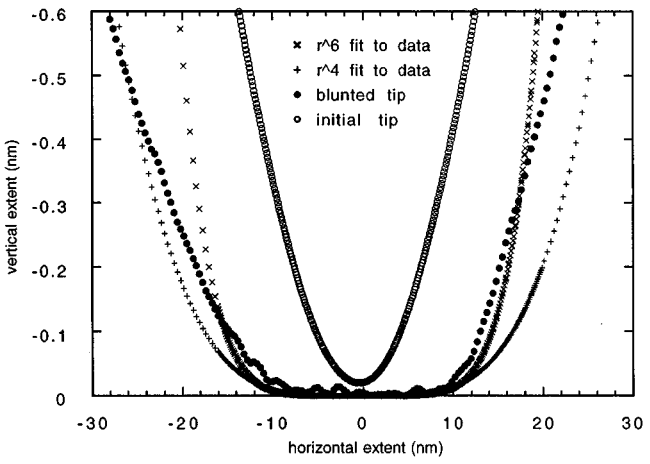

FIG. 4. The tip image of the deliberately blunted tip compared to the original tip, as well as curve fits. The blunted tip is plotted in solid circles, the original tip, from Fig. 2, in open circles. The blunted tip profile is clearly much flatter than the original parabolic tip. Two curve fits, $z \sim r^4$ (open squares) and r^6 (open diamonds), are plotted for comparison. The $z \sim r^6$ curve does the best job fitting the flat tip shape near its end. This is consistent with the extended JKR fit to the friction vs load data.

calculated from recent accurate Brillouin scattering data.[33] It is not unreasonable to apply bulk values for the elastic constants for a nanometer-sized contact, particularly in light of a recent experiment which indicated that the Young's modulus measured in a nanometer-sized Au contact was within experimental error of the macroscopic value.[34]

For the data presented in Fig. 1, we estimate a critical load of 138 nN, with the frictional force at pull off equal to 128 nN. From this, we estimate an interfacial surface energy of 210 mJ/m^2 and a shear strength of 0.86 GPa. The indentation at maximum load is estimated to be 6 Å, where the average pressure is roughly 0.38 GPa at this load. The contact area at pull off is roughly 150 nm^2 for this data, corresponding to a contact radius of 7 nm at pull off.

The interfacial surface energy of 210 mJ/m^2 is an order of magnitude higher than surface energies measured in air with the SFA for hydrocarbon surfaces.[35] For comparison, the interfacial energy per surface of two mica surfaces in contact has been measured with a SFA to be as high as 150 mJ/m^2 in dry nitrogen[36] which is comparable to our measurement. In these SFA experiments, surface energy is seen to decrease due to increased humidity and contamination. The high interfacial surface energy we measure is not surprising considering that in UHV humidity is eliminated and contamination minimized.

Our observations suggest that the shear strength for a nanometer-sized contact is surprisingly large compared to that of bulk metals, but of the same order of magnitude of the ideal shear strength of metals in the absence of dislocations.[37] A method for determining the ultimate shear strength of a metal–ceramic interface was used in the case of a silica–copper interface.[38] The ultimate shear strength was measured to be in the range of 0.56–1.67 GPa, attributed to strong metal–oxide bonds formed at the interface.

Finally, we note that during the course of our experiments with the Pt-coated tip, the adhesion progressively decreased as we continued to scan. The data set presented in Fig. 1 was among the initial sets obtained. This behavior, which we attribute to a change of tip chemistry during scanning, will be discussed in more detail elsewhere.[31] Thus, the values quoted here should not be considered absolute measurements of interfacial energy or shear strength for the Pt-mica interface.

V. SUMMARY

Macroscopic theories agree with experiments that friction is proportional to applied load, where the constant of proportionality is defined as the friction coefficient. These macroscopic situations involve multiple asperity contacts and plastic deformation. Our results demonstrate that the concept of a friction coefficient is not valid in the elastic single-asperity regime for nanometer-sized contacts between mica and Pt measured in UHV. Rather, the frictional force is proportional to the contact area predicted by the JKR theory of elastic adhesive contacts. This indicates that the shear strength is pressure independent in the pressure range we examined. Using the JKR theory, one can calculate interfacial energies and shear strengths, to the extent that the tip dimensions, elastic moduli, and AFM signal calibrations are known. The entire shape of the JKR curves are fixed by selection of one pair of points on the friction-load plot, allowing us to see the difference between a parabolic tip versus a flatter tip that was deliberately blunted. This difference was verified with tip images acquired by scanning sharp ridges on the $SrTiO_3$(305) surface. This establishes that the tip shape and composition are critical in determining the frictional behavior observed in an AFM experiment on a particular surface. Friction measurements with AFM cannot be considered to be fundamental unless these considerations are taken into account.

ACKNOWLEDGMENTS

One of the authors (R.W.C.) acknowledges the support of the Natural Sciences and Engineering Research Council of Canada. A second author (N.A.) acknowledges the support of the Ministry of Education and Science of Spain. The authors would like to thank Alan Lyon for coating the AFM levers with platinum. This work was supported by the Director, Office of Energy Research, Basic Energy Sciences, Materials Division of the US Department of Energy under Contract No. DE-AC03-76SF00098.

APPENDIX: EXTENDED JOHNSON–KENDALL–ROBERTS MODEL

The JKR model can be applied to an axisymmetric tip with height profile $z=c\cdot r^n$. The analytic result expresses the load as a function of contact area as follows:

$$L=-(6\pi\gamma K)^{\frac{1}{2}}(A/\pi)^{\frac{3}{4}}+\tfrac{3}{2}Kcn\Psi(A/\pi)^{(n+1)/2}, \tag{9}$$

where

$$\Psi=\frac{(\frac{n}{2})!^2 2^n}{(n+1)!}, \quad n \text{ even}$$

$$\Psi=\frac{(n+1)!}{\left(\frac{n+1}{2}\right)!^2 2^{n+1}}, \quad n \text{ odd}. \tag{10}$$

The nondimensional form of the equation in terms of the frictional force F_f is given by

$$\hat{L}=-\left(\frac{2n+2}{2n-1}\right)\hat{F}_f^{\frac{3}{4}}+\left(\frac{3}{2n-1}\right)\hat{F}_f{}^{(n+1)/2}, \tag{11}$$

where

$$L_c=-\frac{(2n-1)}{2(n+1)}\left[\frac{(6\pi\gamma)^{n+1}K^{n-2}}{[n(n+1)c\Psi]^3}\right]^{1/(2n-1)}, \tag{12}$$

$$F_c=\tau A_c=\tau\pi\left[\left(\frac{6\pi\gamma}{K}\right)\frac{1}{[n(n+1)c\Psi]^2}\right]^{1/(2n-1)} \tag{13}$$

in analogy to Eqs. (4)–(8).

[1]D. Dowson, *History of Tribology* (Longman, London, 1979).
[2]D. Tabor and R. H. S. Winterton, Proc. R. Soc. London Ser. A **312**, 435 (1969).

[3]J. N. Israelachvili, P. M. McGuiggan, and A. M. Homola, Proc. R. Soc. London Ser. A **331**, 19 (1972).
[4]J. N. Israelachvili, P. M. McGuiggan, and A. M. Homola, Science **240**, 189 (1988).
[5]J. N. Israelachvili, P. M. McGuiggan, and M. L. Gee, Wear **136**, 65 (1990).
[6]J. Krim, E. T. Watts, and J. Digel, J. Vac. Sci. Technol. A **8**, 3417 (1990).
[7]E. T. Watts, J. Krim, and A. Widom, Phys. Rev. B **41**, 3466 (1990).
[8]J. Krim, D. H. Solina, and R. Chiarello, Phys. Rev. Lett. **66**, 181 (1991).
[9]G. Binnig, C. F. Quate, and C. Gerber, Phys. Rev. Lett. **56**, 930 (1986).
[10]C. M. Mate, G. M. McClelland, R. Erlandsson, and S. Chiang, Phys. Rev. Lett. **59**, 1942 (1987).
[11]F. P. Bowden and D. Tabor, *Friction and Lubrication of Solids Part I* (Oxford University Press, Oxford, 1950).
[12]S. Granick, in *Fundamentals of Friction*, edited by I. L. Singer and H. M. Pollock (Kluwer, Dordrecht, 1992).
[13]J. N. Israelachvili, in Ref. 12.
[14]B. J. Briscoe and D. C. B. Evans, Proc. R. Soc. London Ser. A **380**, 389 (1982).
[15]Q. Dai, R. Vollmer, R. W. Carpick, D. F. Ogletree, and M. Salmeron, Rev. Sci. Instrum. **66**, 5266 (1995).
[16]R. W. Carpick, D. F. Ogletree, and M. Salmeron (unpublished).
[17]H. Hertz, J. Reine Angew. Math. **92**, 156 (1881).
[18]K. L. Johnson, K. Kendall, and A. D. Roberts, Proc. R. Soc. London Ser. A **324**, 301 (1971).
[19]D. Maugis and M. Barquins, J. Phys. D **16**, 1843 (1983).
[20]D. Maugis, Langmuir **11**, 679 (1995).
[21]A. M. Homola, J. N. Israelachvili, M. L. Gee, and P. M. McGuiggan, Trans. ASME: J. Tribology **111**, 675 (1989).
[22]Nanoprobe, Digital Instruments, Santa Barbara, CA.
[23]A. L. Bogdanov, D. Erts, B. Nilsson, and H. Olin, J. Vac. Sci. Technol. B **12**, 3681 (1994).
[24]T. O. Glasbey *et al.*, Surf. Sci. **318**, L1219 (1994).
[25]L. Montelius, J. O. Tegenfeldt, and P. van Heeren, J. Vac. Sci. Technol. B **12**, 2222 (1994).
[26]F. Atamny and A. Baiker, Surf. Sci. **323**, L314 (1995).
[27]S. S. Sheiko, M. Möller, E. M. C. M. Reuvekamp, and H. W. Zandbergen, Phys. Rev. B **48**, 5675 (1993).
[28]J. Hu, X.-D. Xiao, D. F. Ogletree, and M. Salmeron, Surf. Sci. **327**, 358 (1995).
[29]A. R. Savkoor, in Ref. 12.
[30]R. W. Carpick, N. Agraït, D. F. Ogletree, and M. Salmeron (unpublished).
[31]R. W. Carpick, N. Agraït, D. F. Ogletree, and M. Salmeron, Langmuir (in press).
[32]*Metals Handbook* (American Society for Metals, Metals Park, OH, 1990).
[33]L. E. McNeil and M. Grimsditch, J. Phys. Condens. Matter **5**, 1681 (1992).
[34]N. Agraït, G. Rubio, and S. Vieira, Phys. Rev. Lett. **74**, 3995 (1994).
[35]J. N. Israelachvili, *Intermolecular and Surface Forces* (Academic, San Diego, CA, 1992).
[36]H. K. Christenson, J. Phys. Chem. **97**, 12034 (1993).
[37]A. Kelly, *Strong Solids* (Oxford University Press, London, 1973).
[38]D. C. Agrawal and R. Raj, Acta Metall. **37**, 1265 (1989).